Correlation Effects on Magnetic Anisotropy in Fe and Ni

Imseok Yang*
Department of Physics and Astronomy and Center for Condensed Matter Theory, Rutgers University, Piscataway, NJ 08854

Sergej Y. Savrasov†
Department of Physics, New Jersey Institute of Technology, Newark, NJ 07102

Gabriel Kotliar‡
Department of Physics and Astronomy and Center for Condensed Matter Theory, Rutgers University, Piscataway, NJ 08854

(Dated: February 1, 2008)

We calculate magnetic anisotropy energy of Fe and Ni by taking into account the effects of strong electronic correlations, spin-orbit coupling, and non-collinearity of intra–atomic magnetization. The LDA+U method is used and its equivalence to dynamical mean–field theory in the static limit is derived. The effects of strong correlations are studied along several paths in (U, J) parameter space. Both experimental magnitude of MAE and direction of magnetization are predicted correctly near $U = 1.9\ eV$, $J = 1.2\ eV$ for Ni and $U = 1.2\ eV$, $J = 0.8\ eV$ for Fe. The modified one–electron spectra by strong correlations are emphasized in conjunction with magnetic anisotropy.

I. INTRODUCTION

One of the long-standing problems that are still short of detailed understanding is to explain the magneto-crystalline anisotropy energy of magnetic materials containing transition-metal elements, especially that of Fe, Co, and Ni. Magnetic anisotropy is the dependency of internal energy on the direction of spontaneous magnetization. Generally, the magnetic anisotropy energy term possesses the symmetry of the crystal. It is therefore called magneto-crystalline anisotropy or crystal magnetic anisotropy. In transition metals, most of the magnetic moment comes from spin polarization. Within the non-relativistic approach, there is no term coupling to the spin degrees of freedom. The magnetic moment, therefore, can points to an arbitrary direction. The magnetic anisotropy energy is an relativistic phenomenon of spin-orbit coupling. With spin-orbit coupling, the spin degrees of freedom interact with the spatial anisotropy through the coupling to the orbital degrees of freedom. This induces a preferred direction of spins. This happens even though the total angular momentum is completely quenched. Since spin-orbit coupling couples individual spin degrees of freedom to individual orbital degrees of freedom, the fact that total orbital magnetic moment is quenched does not affect the visibility of spatial anisotropy to magnetic moment.

The primary difficulty toward investigating MAE has been attributed to the fact that the MAE of the metals are as small as of the order of 1 μeV/atom. At low temperature ($T = 4.2K$), MAE is of the order of 60 μeV/atom for hcp Co, 2.8μeV/atom for fcc Ni, and 1.4 μeV/atom for bcc Fe. With advances in the accurate total energy method combined with the development of faster computers, attempts have been made to calculate MAE from first-principles for bulk crystalline Fe, Co, and Ni. While the magnitude of the MAE have been predicted for all the three metals, the correct easy axis for Ni has not been predicted so far. Here we present new results that predict the correct easy axis for Ni as well as reproduce the previous results in relevant limits. This result is obtained by incorporating spin–orbit coupling, non-collinear nature of of intra–atomic magnetization, and strong correlation effects. We also suggest why the previous approaches have failed in obtaining the correct easy axis for Ni.

Experimentally, there are various ways of measuring the magnetic anisotropy energy. These range from torque measurements, saturation magnetic fields and ferromagnetic resonance methods. However, torque measurements are more often used and are considered to be reasonably precise. The main principle behind the torque experiments is that in the presence of an external magnetic field misaligned with respect to the easy axis (or equivalently, direction of the crystal magnetization), the magnetic moment experiences a torque. In equilibrium, this torque is balanced by the crystal anisotropy torque. Torque magneto–meters are used to precisely measure this torque. Since the crystal anisotropy torque is just the angular derivative of the magnetic anisotropy energy, a measurement of the torque gives an indirect estimate of the anisotropy energy. The torque measured at various angles are interpolated to a corresponding analytic expression such as angular derivatives of total energy. The analytic expression of total energy can be expressed in terms of parameters based on crystal symmetry.

The simplest form of crystal magnetic anisotropy is uniaxial anisotropy, for example, in hexagonal cobalt with easy direction parallel to the c axis of the crystal at room temperature. As the internal magnetization rotates away from the c axis, the anisotropy energy increases with increase of ϕ, where ϕ is the angle between the c axis and the internal magnetization. We can expand this energy in a series of powers of $\sin^2\phi$:

$$E_a = K_1 \sin^2\phi + K_2 \sin^4\phi + \cdots, \tag{1}$$

where K_1 and K_2 are constants.

For cubic crystals such as iron and nickel, the anisotropy energy can be expressed in terms of the directional cosines $(\alpha_1, \alpha_2, \alpha_3)$ of the internal magnetization with respect to the three cubic edges. Because of the high symmetry of the cubic crystal, the anisotropy energy can be expressed in a fairly simple way:

$$E_a = K_1 \left(\alpha_1^2\alpha_2^2 + \alpha_2^2\alpha_3^3 + \alpha_3^2\alpha_1^2\right) + K_2 \left(\alpha_1^2\alpha_2^2\alpha_3^2\right) + \cdots, \tag{2}$$

where K_1 and K_2 are constants.

The constants K_n obtained by interpolating the torque are substituted back to get the expression for the total energy. Magnetic anisotropy energy is calculated by subtracting energies at two different direction of magnetic moments, e.g. [001] and [111]

To measure the torque, specimens are formed into short cylinders. The specimens are mounted in a carriage held by two torsion fibers that are fastened to a rigid support at the top and to a circular scale S at the bottom. When the field is excited in the electromagnet, the crystal tends to turn so that the direction of easy magnetization is parallel to the field. The torque so produced is balanced by turning the bottom of the lower fiber until the crystal regains its original orientation as determined by reflection of a light beam from the mirror. The scale reading S_2 is then compared with the original reading S_1 with $H = 0$. $S_2 - S_1$ is a measure of the torque. The orientation of the crystal axes with respect to the applied field is varied by turning the electromagnet, which is mounted on a heavy bearing, and noting its position on a suitable scale, S'. One then plots the torque against the crystal orientation and deduces from the curve the crystal anisotropy constant K_n.

Early attempts to explain magnetic anisotropy are based on the interaction between the magnetization and the lattice through spin-orbit coupling combined with band theory[1]. Later, Brooks[2] used an itinerant electron model and orbital angular momentum quenching in cubic crystals to explain MAE. Treating the spin-orbit coupling as a perturbation, the nontrivial magnetic anisotropy came out at the fourth-order. The correct directions of magnetization were obtained for Fe and Ni. The difference between easy axes in these metals was attributed to the different lattice structures of them. Based on Ni-Fe alloy data, however, a much closer correlation between the anisotropy and the number of valence electrons was observed. What is the factor that determines the easy axis has been another unanswered question since then. In subsequent papers[3,4,5] the calculations became more and more refined. Finally the discussion centered around the importance of degenerate states along symmetry lines in the Brillouine zone and plausible explanations of the origin of magnetic anisotropy were provided[6,7].

Contemporary studies of magnetic anisotropy energy have centered on first-principles calculations, using density functional theory[8] within the framework of local spin density approximation (LSDA)[9]. Eckardt, Fritsche, and Noffke[10] were able to get the values of the right order of magnitude for Fe and Ni, but with incorrect easy axis for Fe. Daalderop, Kelly, and Schuurmans[11] used the force theorem[12] to obtain the correct order of magnitude of the MAE for Fe, Co, and Ni, but incorrect easy axes were found for Co, and Ni. They also observed that changing the number of valence electrons, hence removing the LDA artificial X_2 pocket would restore the correct easy axis. This observation is similar to Brooks' observation of the close correlation bewteen the direction of magnetic moment and the number of valence electrons. Wang, Wu, and Freeman developed state tracking method to study magnetic anisotropy of Fe[13]. Trygg, Johansson, Eriksson, and Willis[14] improved the method while using fully self-consistent approach. Orbital polarization was also incorporated, which was suggested by Jansen[15]. While the correct easy axis was obtained for Co and Fe, in case of Ni the calculation still gave the wrong easy axis. This is the best result before the current work. Schneider, Erickson, and Jansen[16] used torque instead of energy difference to obtain the same result as that of Trygg, Johansson, Eriksson, and Willis. They also treated the spin-orbit coupling constant as an adjustable parameter. They succeeded in restoring the correct easy axis for Ni with an unphysically large value of spin-orbit coupling. This work suggested a close relation between magnetic anisotropy energy and the strength of spin-orbit coupling. Halilov, Perlov, Oppeneer, Yaresko ,and Antonov also scaled spin-orbit coupling in order to enlarge its effect on the MAE and confirmed previous results[17].

We believe that the physics of transition metal compounds is intermediate between atomic limit where the localized d electrons are treated in the real space and fully itinerant limit when the electrons are described by band theory in k space. A many–body method incorporating these two important limits is the dynamical mean–field theory (DMFT)[18]. The DMFT approach has been extensively used to study model Hamiltonian of correlated electron systems in the weak, strong and intermediate coupling regimes. It has been very successful in describing the physics of realistic systems, like the transition metal oxides and, therefore, is expected to treat properly the materials with d or f electrons.

We take a new view that the correlation effects within the d shell are important for the magnetic anisotropy of $3d$ transition metals like Ni. These effects are not captured by the LDA but are described by Hubbard–like interactions presented in these systems and need to be treated by an extension of first principles methods such as DMFT. Since, DMFT reduces to LDA+U[19] in static limit, we adopt LDA+U method to attack the problem of magnetic anisotropy of $3d$ transition metals.

Another effect which has not been investigated in the context of magnetic anisotropy calculations is the non-collinear nature of intra-atomic magnetization[20]. It is expected to be important when spin-orbit coupling and correlation effects come into play together. We show that when we include these new ingredients into the calculation we solve the long-standing problem of predicting the correct easy axis of Ni. Part of this work has been pub-

lished elsewhere[21].

The remainder of this paper is organized as follows. Section II presents DMFT extended to relativistic electron structure problem, its equivalence to LDA+U in static limit. Section III describes calculated MAE. Section IV discusses the calculated MAE in conjunction with band structure. Section V presents how to include other relativistic corrections than spin–orbit coupling and discuss the effects of spin–other–orbit coupling. Section VI is a summary and conclusion.

II. DMFT AND LDA+U

The LDA method is very successful in many materials for which the one–electron model of solids works. However, in correlated electron system this is not always the case. In strongly correlated situations, the total energy is not very sensitive to the potential since the electrons are localized due to the interactions themselves, and the lack of sensitivity of the functional to the density, does not permit to devise good approximations to the exact functional in this regime. For example, when the Mott transition takes place the invertibility condition is not satisfied. Our view is that these difficulties cannot be remedied by using more complicated exchange and correlation functionals in density functional theory. DMFT is a method successfully describing strongly correlated systems[18] and has been extended to electronic structure problems[22]. In this work we utilize the new functional formulation of the electronic structure problem and extend it to relativistic case.

The basic idea is to introduce another relevant variable in addition to the density ρ and the magnetic moment density $\mathbf{m}$, namely the local Green function. The latter is defined by projecting the full Green function onto a separate subset of correlated "heavy" orbitals distinguished by the orbital index a and the spin index σ from a complete set of orbitals $\chi_a^\sigma(\mathbf{r}-\mathbf{R}) \equiv \chi_{aR}^\sigma$ of a tight-binding representation which we assume for simplicity to be orthogonal. The local Green function is therefore given by a matrix $\hat{G}$ with elements[23]

$$G_{ab}^{\sigma\sigma'}(i\omega,\mathbf{R}) = -\left\langle c_{aR}^{\sigma}(i\omega)c_{bR}^{\sigma'+}(i\omega)\right\rangle = \tag{3}$$
$$-\int \chi_a^{\sigma*}(\mathbf{r}-\mathbf{R})\left\langle\psi(\mathbf{r},i\omega)\psi^+(\mathbf{r}',i\omega)\right\rangle\chi_b^{\sigma'}(\mathbf{r}'-\mathbf{R})d\mathbf{r}d\mathbf{r}'.$$

We then construct a functional $\Gamma[\,\rho,\mathbf{m},\hat{G}\,]$ which gives the exact free energy at a stationary point.

To describe the new method, we consider fermion system under an external potential $V_{\rm ext}$ and an external magnetic field $\mathbf{h}$. For relativistic effects spin-orbit coupling, whose effects are important for magnetic anisotropy calculations, are also considered. Spin-orbit coupling is included according to the suggestion by Andersen[24]. It is useful to introduce the notion of the Kohn-Sham potential $V_{\rm KS}$, the Kohn-Sham magnetic field $\mathbf{h}_{\rm KS}$ and its dynamical analog $\Sigma_{ab}^{\sigma\sigma'}(i\omega_n)$. They are defined as the functions that one needs to add to the kinetic energy matrix so as to obtain a given density and spectral function of the heavy orbitals namely:

$$\rho(\mathbf{r}) = T\sum_{i\omega_n}\mathrm{Tr}_s\left\langle\mathbf{r}s\left|[(i\omega_n+\nabla^2/2-V_{\rm KS})\mathrm{I}\right.\right.$$
$$\left.\left.-\,2\mu_B\mathbf{s}\cdot\mathbf{h}_{\rm KS}-\xi(\mathbf{r})\mathbf{l}\cdot\mathbf{s}-\Sigma]^{-1}\right|\mathbf{r}s\right\rangle e^{i\omega_n 0^+} \tag{4}$$
$$\mathbf{m}(\mathbf{r}) = -2\mu_B T\sum_{i\omega_n}\mathrm{Tr}_s\left\langle\mathbf{r}s\left|\mathbf{s}[(i\omega_n+\nabla^2/2-V_{\rm KS})\mathrm{I}\right.\right.$$
$$\left.\left.-2\mu_B\mathbf{s}\cdot\mathbf{h}_{\rm KS}-\xi(\mathbf{r})\mathbf{l}\cdot\mathbf{s}-\Sigma]^{-1}\right|\mathbf{r}s\right\rangle e^{i\omega_n 0^+} \tag{5}$$

where Tr_s is the trace over spin space, $\mathbf{l}$ and $\mathbf{s}$ are one-electron orbital and spin angular momentum operator, respectively. The spin angular momentum operator is expressed in terms of Pauli matrices $\mathbf{s} = \vec{\sigma}/2$ and I is 2×2 unit matrix. V_{KS} and $\mathbf{h}_{\rm KS}$ are functions of $\mathbf{r}$. The chemical potential μ is set to zero throughout the current section, and Σ is given by

$$\Sigma \equiv \Sigma(\mathbf{r},\mathbf{r}',i\omega) = \sum_{ab\sigma\sigma' R}\chi_a^{\sigma*}(\mathbf{r}-\mathbf{R})\Sigma_{ab}^{\sigma\sigma'}(i\omega)\chi_b^{\sigma'}(\mathbf{r}'-\mathbf{R}). \tag{6}$$

$\xi(\mathbf{r})$ determines the strength of spin–orbit coupling and in practice is determined[25] by radial derivative of the $l=0$ component of the Kohn–Sham potential inside an atomic sphere:

$$\xi(r) = \frac{2}{c^2}\frac{dV_{\rm KS}(r)}{dr}. \tag{7}$$

When spin–orbit coupling is present, the intra–atomic magnetization $\mathbf{m}(\mathbf{r})$ is not collinear, i.e., the direction of magnetization depends on the position $\mathbf{r}$. Therefore, the magnetization must be treated as a general vector field, which realizes non-collinear intra-atomic nature of this quantity. Such general magnetization scheme has been recently discussed[20]

In terms of these quantities and the matrix of local interactions $\hat{U}$, we write down the DMFT+LSDA functional:

$$\Gamma_{\rm LSDA+DMFT}(\rho,V_{\rm KS},\mathbf{m},\mathbf{h}_{\rm KS},\hat{G},\hat{\Sigma}) =$$
$$-T\sum_{\omega}e^{i\omega 0^+}\mathrm{Tr}\log[(i\omega+\nabla^2-V_{\rm KS})\mathrm{I}-2\mu_B\mathbf{s}\cdot\mathbf{h}_{\rm KS}$$
$$-\xi(\mathbf{r})\mathbf{l}\cdot\mathbf{s}-\Sigma] - \int d\mathbf{r}V_{KS}(\mathbf{r})\rho(\mathbf{r}) + \int d\mathbf{r}\mathbf{m}(\mathbf{r})\cdot\mathbf{h}_{\rm KS}(\mathbf{r})$$
$$-\sum_{\omega}e^{i\omega 0^+}\mathrm{Tr}[\hat{\Sigma}(i\omega)\hat{G}(i\omega)] + \int d\mathbf{r}V_{ext}(\mathbf{r})\rho(\mathbf{r})$$
$$-\int d\mathbf{r}\mathbf{h}(\mathbf{r})\cdot\mathbf{m}(\mathbf{r}) + \frac{1}{2}\int d\mathbf{r}d\mathbf{r}'\frac{\rho(\mathbf{r})\rho(\mathbf{r}')}{|\mathbf{r}-\mathbf{r}'|}$$
$$+E_{\rm xc}^{\rm LSDA}[\rho,\mathbf{m}] + \sum_R[\Phi[\hat{G}]-\Phi_{DC}]. \tag{8}$$

$\Phi[\hat{G}]$ is the sum of the two–particle irreducible local diagrams constructed with the local interaction matrix $\hat{U}$, and the local heavy propagator $\hat{G}$. Φ_{DC} is the so–called

double counting term which subtracts the average energy of the heavy level already described by LDA. Expression (8) ensures that the Greens function obtained from its extremization will satisfy the Luttinger theorem.

$E_{\rm xc}^{\rm LSDA}[\rho,\mathbf{m}]$ is the LSDA exchange correlation energy. Since the exact exchange correlation energy functional is not known, the usefulness of this approach is due to the existence of successful approximations to the exchange correlation energy functional as Kohn and Sham proposed. When nontrivial magnetic moment is present, the exchange correlation energy functional is assumed to be dependent on density and magnetization:

$$E_{\rm xc}^{\rm LSDA}[\rho,\mathbf{m}] = \int d\mathbf{r}\epsilon_{\rm xc}[\rho(\mathbf{r}),m(\mathbf{r})]\rho(\mathbf{r}) \quad (9)$$

$$+ \int d\mathbf{r} f_{\rm xc}[\rho(\mathbf{r}),m(\mathbf{r})]m(\mathbf{r})(\mathbf{r}), \quad (10)$$

where $m=|\mathbf{m}|$.

The functional (8) can be viewed as a functional of six independent variables, since the stationary condition in the conjugate fields reproduces the definition of the dynamical potential and the Weiss field. Extremizing it with respect $V_{\rm KS}$, $\mathbf{h}_{\rm KS}$, and Σ lead us to compute the density(Eq. (4)), the magnetic moment density(Eq. (5)), and the Green function $G_{ab}^{\sigma\sigma'}(i\omega)$ (Eq. (14)), respectively. The Kohn–Sham potential $V_{\rm KS}(\mathbf{r})$ and Kohn–Sham magnetic field $\mathbf{h}_{\rm KS}(\mathbf{r})$ are obtained by extremizing the functional with respect to $\rho(\mathbf{r})$ and $\mathbf{m}(\mathbf{r})$:

$$V_{\rm KS}(\mathbf{r}) = V_{\rm ext}(\mathbf{r}) + \int d\mathbf{r}'\frac{\rho(\mathbf{r}')}{|\mathbf{r}-\mathbf{r}'|} + \frac{\delta E_{\rm xc}^{\rm LDA}[\rho,\mathbf{m}]}{\delta\rho(\mathbf{r})} \quad (11)$$

$$\mathbf{h}_{\rm KS}(\mathbf{r}) = \mathbf{h}(\mathbf{r}) + \frac{\delta E_{\rm xc}^{\rm LDA}[\rho,\mathbf{m}]}{\delta\mathbf{m}(\mathbf{r})}. \quad (12)$$

Extremizing with respect to $G_{ab}^{\sigma\sigma'}$ yields the equation for self energy

$$\Sigma_{ab}^{\sigma\sigma'}(i\omega) = \frac{\delta\Phi}{\delta G_{ab}^{\sigma\sigma'}(i\omega)} - \frac{\delta\Phi_{DC}}{\delta G_{ab}^{\sigma\sigma'}(i\omega)}. \quad (13)$$

The physical meaning of the dynamical potential Σ is parallel to the meaning of the original Kohn-Sham potential $V_{\rm KS}$: it is the function that one needs to add to the correlated block of the one-electron Hamiltonian in order to obtain the desired local Green function:

$$G_{ab}^{\sigma\sigma'}(i\omega) = \sum_{\mathbf{k}}[i\omega - \hat{H}^{\mathbf{k}} - \hat{\Sigma}(i\omega)]_{ab}^{\sigma\sigma'-1}, \quad (14)$$

where $H_{ab}^{\sigma\sigma'\mathbf{k}} = \langle\chi_{a\mathbf{k}}^{\sigma}|(-\nabla^2+V_{\rm KS})\mathrm{I} + 2\mu_B\mathbf{s}\cdot\mathbf{h}_{\rm KS} + \xi(\mathbf{r})\mathbf{l}\cdot\mathbf{s}|\chi_{b\mathbf{k}}^{\sigma'}\rangle$ is the one-electron Hamiltonian in $\mathbf{k}$-space. It is the frequency dependence of the dynamical potential which allows us to treat Hubbard bands and quasiparticle bands on the same footing.

In general, an explicit form of $\Phi[G]$ is not available. DMFT maps the DMFT+LSDA function to an Anderson impurity model. Self–consistency equations obtained in this way are used to find the self energy (13). In this paper we confine ourselves to zero temperature and make an additional assumption on solving the impurity model using the Hartree–Fock approximation. In this limit an explicit form of $\Phi[G]$ is available and DMFT self–consistency loop is unnecessary. We first figure out the Coulomb interaction by considering a Hartree–Fock averaging of the original expression for the Coulomb interaction given by

$$\frac{1}{2}\sum_{\sigma\sigma'}\sum_{abcd}\langle a\sigma b\sigma'|\frac{e^2}{r}|c\sigma d\sigma'\rangle c_a^{\sigma+}c_b^{\sigma'+}c_d^{\sigma'}c_c^{\sigma}. \quad (15)$$

In this limit, the sum of local graphs reduce to

$$\Phi[\hat{G}] = \frac{1}{2}\sum_{abcd\sigma}U_{abcd}n_{ab}^{\sigma\sigma}n_{cd}^{-\sigma-\sigma} + \frac{1}{2}\sum_{abcd\sigma}(U_{abcd}-J_{abcd})n_{ab}^{\sigma\sigma}n_{cd}^{\sigma\sigma} - \frac{1}{2}\sum_{abcd\sigma}J_{abcd}n_{ab}^{\sigma-\sigma}n_{cd}^{-\sigma\sigma}. \quad (16)$$

Here, the matrices $U_{abcd} = \langle ac|v_C|bd\rangle$ and $J_{abcd} = \langle ac|v_C|db\rangle$ have the following definitions:

$$U_{abcd} = \int\chi_a^{\sigma*}(\mathbf{r})\chi_c^{\sigma*}(\mathbf{r}')v_C(\mathbf{r}-\mathbf{r}')\chi_b^{\sigma}(\mathbf{r})\chi_d^{\sigma}(\mathbf{r}')d\mathbf{r}d\mathbf{r}',$$

$$J_{abcd} = \int\chi_a(\mathbf{r})^{\sigma*}\chi_c^{\sigma*}(\mathbf{r}')v_C(\mathbf{r}-\mathbf{r}')\chi_d^{\sigma}(\mathbf{r})\chi_b^{\sigma}(\mathbf{r}')d\mathbf{r}d\mathbf{r}',$$

where the Coulomb interaction $v_C(\mathbf{r}-\mathbf{r}')$ has to take into account the effects of screening by conduction electrons. Note that the matrices U_{abcd} and J_{abcd} are spin independent since the Coulomb interaction is independent of spin. The occupancy matrix $n_{ab}^{\sigma\sigma'}$ is a derived quantity of the Green function:

$$n_{ab}^{\sigma\sigma'} = T\sum_{\omega}G_{ab}^{\sigma\sigma'}(i\omega)e^{i\omega 0^+}. \quad (17)$$

Notice that when spin–orbit coupling is taken into account, the occupancy matrix becomes non–diagonal with respect to spin index even though the interaction matrices U_{abcd} and J_{abcd} are spin independent.

The self energy $\Sigma_{ab}^{\sigma\sigma'}$ now takes the from for spin diagonal elements

$$\Sigma_{ab}^{\sigma\sigma} = \sum_{cd}U_{abcd}n_{cd}^{-\sigma-\sigma} + \sum_{cd}(U_{abcd}-J_{abcd})n_{cd}^{\sigma\sigma} - \frac{\delta\Phi_{DC}}{\delta G_{ab}^{\sigma\sigma}(i\omega)}, \quad (18)$$

and for spin off–diagonal elements it is given by

$$\Sigma_{ab}^{\sigma-\sigma} = -\sum_{cd}J_{abcd}n_{cd}^{-\sigma\sigma} - \frac{\delta\Phi_{DC}}{\delta G_{ab}^{\sigma-\sigma}(i\omega)}. \quad (19)$$

The off–diagonal elements of the self energy only present when spin–orbit coupling is included, hence a relativistic

effect. To make it more physically transparent we can introduce magnetic moments at the given shell by

$$m^{\mu}_{ab} = \sum_{\sigma\sigma'} s^{\mu}_{\sigma\sigma'} n^{\sigma\sigma'}_{ab} \quad (20)$$

where μ runs over x, y, z for Cartesian coordinates, or over,$-1, 0, +1$ $(z, \pm)$ for spherical coordinates. Relativistic correction from strong correlations can be written in physically transparent form

$$\begin{aligned} \frac{1}{2}\sum_{abcd\sigma} J_{abcd} n^{\sigma-\sigma}_{ab} n^{-\sigma\sigma}_{cd} &\equiv \frac{1}{2}\sum_{abcd} m^{(+)}_{ab} J_{abcd} m^{(-)}_{cd} \\ &+ \frac{1}{2}\sum_{abcd} m^{(-)}_{ab} J_{abcd} m^{(+)}_{cd} \quad (21) \end{aligned}$$

and in principle has room for further generalization of exchange matrix J_{abcd} to be anisotropic, i.e depend on $\mu\mu'$: $J^{\mu\mu'}_{abcd}$.

Part of the energy added by $\Phi[\hat{G}]$ is already included in LSDA functional. The double counting term $\Phi_{\rm dc}$ is added to subtract this already included part of $\Phi[\hat{G}]$. It was proposed[26] that the form for $\Phi[\hat{G}]$ is

$$\Phi^{\rm Model}_{\rm dc} = \frac{1}{2}\bar{U}\bar{n}(\bar{n}-1) - \frac{1}{2}\bar{J}[\bar{n}^{\uparrow}(\bar{n}^{\uparrow}-1) + \bar{n}^{\downarrow}(\bar{n}^{\downarrow}-1)], \quad (22)$$

where

$$\begin{aligned} \bar{U} &= \frac{1}{(2l+1)^2}\sum_{ab}\langle ab|\frac{1}{r}|ab\rangle, \quad (23) \\ \bar{J} &= \bar{U} - \frac{1}{2l(2l+1)}\sum_{ab}(\langle ab|\frac{1}{r}|ab\rangle - \langle ab|\frac{1}{r}|ba\rangle), \quad (24) \end{aligned}$$

and $\bar{n}^{\sigma} = \sum_a n^{\sigma}_{aa}$, and $\bar{n} = \bar{n}^{\uparrow} + \bar{n}^{\downarrow}$. The subtraction by 1 is made to take the self-interaction into account. This generates the self energy in the form:

$$\begin{aligned} \Sigma^{\sigma\sigma}_{ab} &= \sum_{cd} U_{abcd} n^{-\sigma-\sigma}_{cd} + \sum_{cd}(U_{abcd} - J_{abcd}) n^{\sigma\sigma}_{cd} \\ &- \delta_{ab}\bar{U}(\bar{n} - \frac{1}{2}) + \delta_{ab}\bar{J}(\bar{n}^{\sigma} - \frac{1}{2}) \quad (25) \\ \Sigma^{\sigma-\sigma}_{ab} &= -\sum_{cd} J_{abcd} n^{-\sigma\sigma}_{cd}. \quad (26) \end{aligned}$$

As an example, when only the effect of U is under investigation, the U and J matrices are $U_{abcd} = \delta_{ab}\delta_{cd}U$, $J_{abcd} = \delta_{ad}\delta_{cb}U$, $\bar{U} = U$, and $\bar{J} = 0$. This simple U and J matrices make it possible to write down corrections to LSDA functional and LSDA Kohn-Sham potential:

$$\begin{aligned} \Phi[\hat{G}] - \Phi^{\rm Model}_{\rm dc} &= -\frac{1}{2}\sum_{\sigma}\sum_{ab} U(n^{\sigma\sigma}_{ab} n^{\sigma\sigma}_{ba} + n^{\sigma-\sigma}_{ab} n^{-\sigma\sigma}_{ba}) \\ &- \frac{1}{2}U\bar{n} \quad (27) \end{aligned}$$

$$\begin{aligned} \Sigma^{\sigma\sigma}_{ab} &= U(\frac{1}{2}\delta_{ab} - n^{\sigma\sigma}_{ba}) \quad (28) \\ \Sigma^{\sigma-\sigma}_{ab} &= U n^{-\sigma\sigma}_{ba} \quad (29) \end{aligned}$$

The DMFT self consistency equation identifies the Green function of the original model and the Green function of the mapped impurity model to find the self energy. Now that we can express the sum of local graphs $\Phi[\hat{G}]$ in terms of the original Green function, the DMFT loop need not to be performed. The problem is now reduced to extremizing the functional [Eq. (8)] with the expression for the sum of local graphs [Eq. (16)], which is exactly the LDA+U method[19].

The DMFT functional and its static correspondent LDA+U functional are defined once a set of projectors $\{\chi^{\sigma}_{a}(\mathbf{r})\}$ and a matrix of interactions U_{abcd} and J_{abcd} are prescribed. When l orbitals are used as the projection operators, the matrix is expressed in terms of Slater parameters F^k. For $a \equiv lm, b \equiv lk, c \equiv l'm', d \equiv l'k'$ and representing $\chi^{\uparrow}_{a}(\mathbf{r}) = \phi_{lm}(\mathbf{r})(1,0)^{\rm T}$, where $\phi_{lm}(\mathbf{r}) = \phi_l(r) i^l Y_{lm}(\hat{r})$, we can express the matrices U_{abcd} and J_{abcd} in the following manner:

$$\begin{aligned} \langle lml'm'|\frac{1}{r}|lkl'k'\rangle &= \sum_{l''=0,2,\ldots}^{\min(2l,2l')} \frac{4\pi}{2l''+1} F^{(u)l''}_{ll'} \quad (30) \\ &\times (-1)^{m''} C^{l''m''=m-k}_{lklm} C^{l''m''=k'-m'}_{l'm'l'k'} \\ \langle lml'm'|\frac{1}{r}|l'k'lk\rangle &= \sum_{l''=0,2,\ldots}^{\min(2l,2l')} \frac{4\pi}{2l''+1} F^{(j)l''}_{ll'} \quad (31) \\ &\times (-1)^{m''} C^{l''m''=m-k'}_{l'k'lm} C^{l''m''=k-m'}_{l'm'lk} \end{aligned}$$

where the quantities $C^{L''}_{LL'}$ are the Gaunt coefficients which are the integrals of the products of three spherical harmonics

$$C^{L''}_{LL'} = \int Y_L(\hat{\mathbf{r}}) Y^*_{L'}(\hat{\mathbf{r}}) Y_{L''}(\hat{\mathbf{r}}) d\hat{\mathbf{r}}. \quad (32)$$

The quantities $F^{(u)}$ and $F^{(j)}$ are given by the following radial integrals

$$\begin{aligned} F^{(u)l''}_{ll'} &= \int \frac{r^{l''}}{r^{l''+1}} \phi^2_l(r)\phi^2_{l'}(r') dr dr' \quad (33) \\ F^{(j)l''}_{ll'} &= \int \frac{r^{l''}}{r^{l''+1}} \phi_l(r)\phi_{l'}(r)\phi_l(r')\phi_{l'}(r') dr dr'. \quad (34) \end{aligned}$$

When $l \equiv l'$, the quantites $F^{(u)}$ and $F^{(j)}$ are equal and have a name of Slater integrals which for s–electrons are reduced to one constant $F^{(0)}$, for p–electrons there are two constants: $F^{(0)}$, $F^{(2)}$, for d's: $F^{(0)}$, $F^{(2)}$, $F^{(4)}$, etc. In this case, the expressions for U and J are reduced to

$$\langle m, m''|v_C|m', m'''\rangle = \sum_k a_k(m, m', m'', m''') F^k, \quad (35)$$

where $0 \le k \le 2l$, and

$$\begin{aligned} &a_k(m, m', m'', m''') = \\ &\frac{4\pi}{2k+1}(-1)^q C^{kq=m-m'}_{lmlm'} C^{kq=m'''-m''}_{lm''lm'''}. \quad (36) \end{aligned}$$

Slater integrals can be linked to Coulomb and Stoner parameters U and J obtained from LSDA supercell procedures via $U = F^0$ and $J = (F^2 + F^4)/14$. The ratio F^2/F^4 is to a good accuracy a constant ~ 0.625 for d electrons. For f electrons, the corresponding expression is $U = F^0$ and $J = (286F^2 + 195F^4 + 250F^6)/6435$.

To summarize, we have shown the equivalence of Hartree–Fock approximation of DMFT and LDA+U method. LDA+U is the method proposed to overcome the difficulties of LDA when strong correlations are present[27]. Since the density uniquely defines the Kohn–Sham orbitals, and they in turn, determine the occupancy matrix of the correlated orbitals, once a choice of correlated orbitals is made, we still have a functional of the density alone. However it is useful to proceed with Eq. (8), and think of the LDA + U functional as a functional of ρ, $V_{\rm KS}$, $\mathbf{m}$, $\mathbf{h}_{\rm KS}$, $G^{\sigma\sigma'}_{ab}$, and $\Sigma^{\sigma\sigma'}_{ab}$, whose minimum gives better approximations to the ground–state energy in strongly correlated situations. Allowing the functional to depend on the projection of the Kohn–Sham energies onto a given orbital, allows the possibility of orbitally ordered states. This is a major advance over LDA in situations where this orbital order is present. As recognized many years ago, this is a very efficient way of gaining energy in correlated situations, and is realized in a wide variety of systems.

III. NUMERICAL CALCULATION OF MAE

We calculate MAE by taking the difference of two total energies with different directions of magnetization [MAE=$E(111) - E(001)$]. The total energies are obtained via fully self consistent solutions. Since the total energy calculation requires high precision, full potential LMTO method[28] has been employed. For the $\vec{k}$ space integration, we follow the analysis given by Trygg and co–workers[14] and use the special point method[29] with a Gaussian broadening[30] of 15 mRy. The validity and convergence of this procedure has been tested in their work [14]. For convergence of the total energies within desired accuracy, about 15000 k-points per Brillouine zone are needed. We used 28000 k-points to reduce possible numerical noise, while the convergency is tested up to 84000k-points. Our calculations include non-spherical terms of the charge density and potential both within the atomic spheres and in the interstitial region[28]. All the low-lying semi-core states are treated together with the valence states in a common Hamiltonian matrix in order to avoid unnecessary uncertainties. These calculations are spin polarized and assume the existence of long-range magnetic order. Spin-orbit coupling is implemented according to the suggestions by Andersen[24]. We also treat magnetization as a general vector field, which realizes non-collinear intra-atomic nature of this quantity. Such general magnetization scheme has been recently discussed[20].

We first test our method in case of LDA ($U = J = 0$). To compare with previous calculations, we turn off the non-collinearity of magnetization which makes it collinear with the quantization axis. The calculation gives correct orders of magnitude for both fcc Ni ($0.5\ \mu eV$) and bcc Fe ($0.5\ \mu eV$) but with the wrong easy axis for Ni, which is the same result as the previous one[14]. Turning on the non-collinearity results in a a larger value of the absolute value of the MAE ($2.9\ \mu eV$) for Ni but the easy axis predicted to be (001) which is still wrong. The magnitude of the experimental MAE of Ni is $2.8\ \mu eV$ and the easy axis is aligned along (111) direction[31]. For Fe, the non-collinearity of magnetization changes neither MAE ($0.5\ \mu eV$) nor the easy axis (001) from the collinear result. The magnitude of the experimental MAE of Fe is $1.4\ \mu eV$ and the easy axis is aligned along (001) direction.

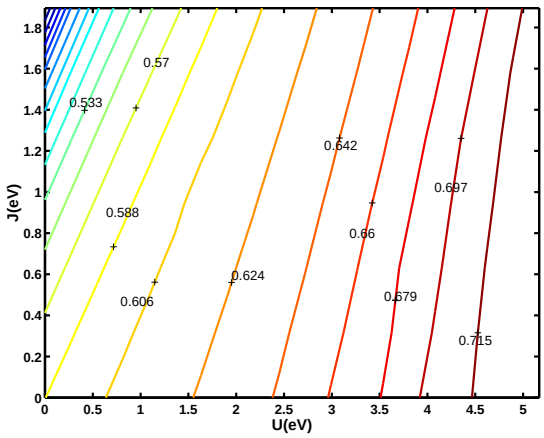

FIG. 1: Ni. Contour plot of magnetic moment as a function of U and J. The contour is drawn at 0.018 $\mu_{\rm B}$ interval, which is 2.9% of the experimental value of magnetic moment 0.606 $\mu_{\rm B}$.

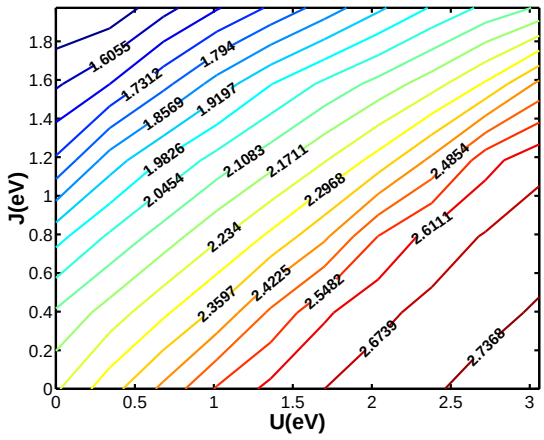

FIG. 2: Fe. Contour plot of magnetic moment as a function of U and J. The contour is drawn at 0.063 $\mu_{\rm B}$ interval, which is 2.9% of the experimental value of magnetic moment 2.2 $\mu_{\rm B}$.

We now describe the effect of correlations, which is crucial in predicting the correct axis of Ni. We first study

the effects of strong correlations on magnetic moments. We have scanned the (U, J) parameter space to obtain magnetic moment as a function of U and J (see Figs. 1 and 2). Magnetic moment increases as U increases, but decreases as J increases for both Ni and Fe. The magnetic moments of Ni and Fe change up to 20% in the parameter range. Notice that well–defined contours exist where the magnetic moments are close to experimental values for both Ni and Fe. In comparison, the magnetic moment of Fe depends more strongly on J than that of Ni. This result is in agreement with an earlier work[32].

We now discuss our calculated MAE. The load of computing MAE is very heavy. Rather than calculating the quantities in the (U, J) parameter space, we follow three paths: two paths with constant J, and the path with experimental magnetic moments.

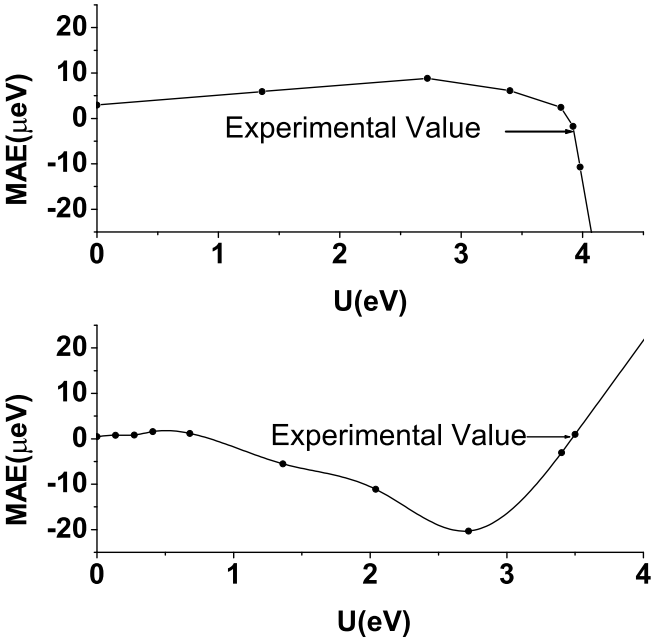

FIG. 3: The magneto–crystalline anisotropy energy MAE = $E(111) - E(001)$ for Ni (top) and Fe (bottom) as functions of U. The experimental MAEs are marked by arrows for Fe ($1.4\ \mu eV$) and Ni ($-2.8\ \mu eV$). The value of J is held to 0.

We first walk along a path with $J = 0\ eV$. For Ni (see Fig. 3), as U increases, the MAE of Ni smoothly increases until U reaches $2.5\ eV$ and then smoothly decreases up to the value $3.8\ \mu eV$. Around $U = 3.9\ eV$, the MAE decreases abruptly to negative value. Around $U = 4.0\ eV$, the experimental order of magnitude and the correct easy axis (111) are restored. The change from the wrong easy axis to the correct easy axis occurs over the range of $\delta U \sim 0.2eV$, which is the order of spin-orbit coupling constant ($\sim 0.1eV$).

For Fe, the MAE decreases on increasing U to negative values, where the magnetization takes the wrong axis. From $U = 2.7\ eV$, it increases back to the correct direction of easy axis (positive MAE). Around $U = 3.5\ eV$, it restores the correct easy axis and the experimental value of MAE is reproduced.

In this study on effects of intra–atomic repulsion, we see that it is possible to predict the correct magnetic anisotropy at a nontrivial U. Notice, however, that the calculated magnetic moments are about 20% larger than those of experiments for both Ni and Fe. As seen in the Figs. 1 and 2, the magnetic moment decreases as J increases. This lead us to follow a path with nontrivial J.

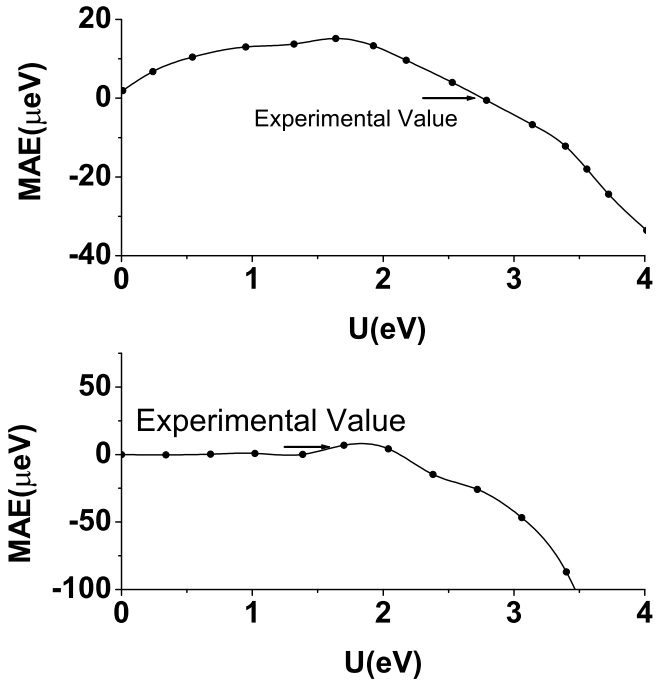

FIG. 4: The magneto–crystalline anisotropy energy MAE = $E(111) - E(001)$ for Ni (top) and Fe (bottom) as functions of U. The experimental MAEs are marked by arrows for Fe ($1.4\ \mu eV$) and Ni ($-2.8\ \mu eV$). The values of J are fixed to 0.9 for both Ni and Fe.

We pick $J = 0.9\ eV$ that seems to be a canonical value of J. For Ni, (see Fig. 4), as U increases, MAE increases to $15\ \mu eV$ till $U = 1.6\ eV$. Then MAE decreases, changing the easy axis from (001) to (111) at $U = 2.6\ eV$. The experimental value of MAE with the correct easy axis is predicted at $2.7\ eV$.

For Fe, MAE increases to $10\ \mu eV$ till $U = 1.9\ eV$. Then MAE decreases, changing the easy axis to (111) direction at $U = 2.2\ eV$. The experimental value of MAE with the correct easy axis is predicted at $1.7\ eV$.

In this study of effects of intra–atomic repulsion (U) with nontrivial J, we are also able to predict the correct magnetic anisotropy at a nontrivial U, much less than that of the case with trivial J. Notice that the calculated magnetic moments are about 5% larger than those of experiments, a big improvement over the case with $J = 0$.

To treat properly the correlation effects on calculated anisotropy energy, the intra–atomic repulsion U and exchange J should be taken into account spontaneously. We, therefore, follow a path in (U, J) space determined by fixed values of magnetic moments close to experimental value.

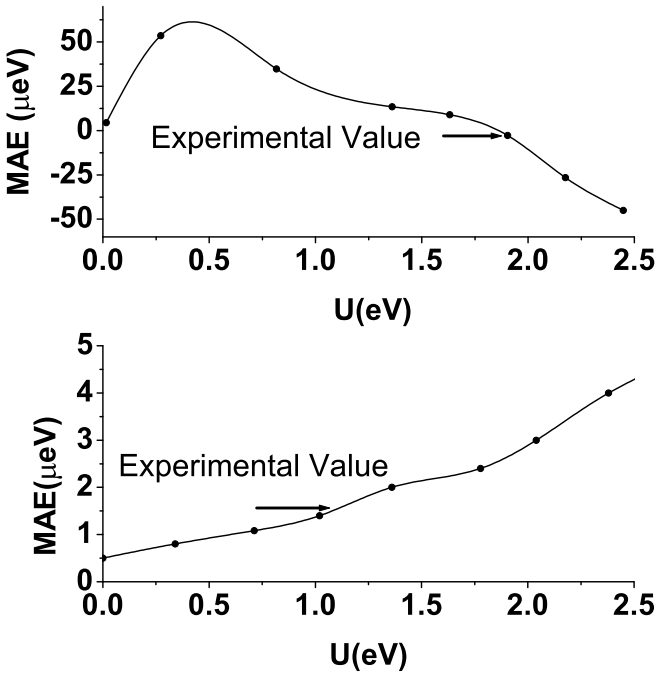

FIG. 5: The magneto–crystalline anisotropy energy MAE = $E(111) - E(001)$ functions of U. The experimental MAEs are marked by arrows for Fe (1.4 μeV) and Ni (-2.8 μeV). The values of exchange parameter J for every value of U are chosen to hold the magnetic moment of 0.61 μ_B in Ni and 2.2 μ_B in Fe

For Ni, we walked along the path of parameters U and J which hold the magnetic moment to 0.61 μ_B. The MAE first increases to 60 μeV ($U = 0.5$ eV, $J = 0.3$ eV) and then decreases (see Fig. 5). While decreasing it makes a rather flat area from $U = 1.4$ eV, $J = 0.9$ eV to $U = 1.7$ eV, $J = 1.1$ eV where MAE is positive and around 10 μeV. After the flat area, the MAE changes from the wrong easy axis to the correct easy axis. The correct magnetic anisotropy is predicted at $U = 1.9$ eV and $J = 1.2$ eV. The change from the wrong easy axis to the correct easy axis occurs over the range of $\delta U \sim 0.2eV$, which is of the order of spin-orbit coupling constant ($\sim 0.1eV$).

For Fe, the MAE is calculated along the path of U and J values where the magnetic moment is fixed to 2.2 μ_B. At $U = 0$ eV and $J = 0$ eV, the MAE is 0.5 μeV. It increases as we move along the contour in the direction of increasing U and J. The correct MAE with the correct direction of magnetic moment is predicted at $U = 1.2$ eV and $J = 0.8$ eV.

In this study of effects of U and J, it is again possible to predict the correct magnetic anisotropy. What is more is that the magnetic moment comes out to be the experimental values at the same time.

We have demonstrated that it is possible to perform highly precise calculation of the total energy in order to obtain both the correct easy axes and the magnitudes of MAE for Fe and Ni. This has been accomplished by including the strong correlation effects via taking intra–atomic repulsion and exchange into account, and incorporating the non–collinear magnetization.

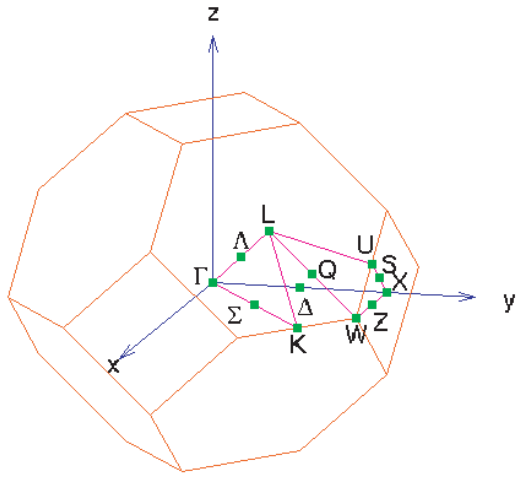

FIG. 6: Brillouine Zone of fcc crystal structure.

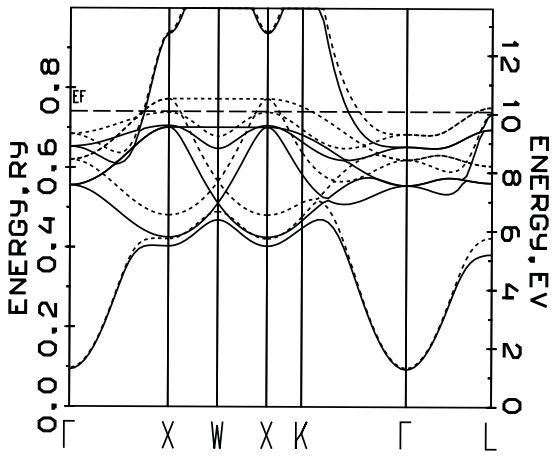

FIG. 7: Calculated band structure of Ni at $U = 1.9$ eV and $J = 1.2$ eV. The solid and dotted lines correspond to majority and minority dominant spin carriers.

IV. MAE AND BAND STRUCTURE

We now present implications of our results on the calculated electronic structure for Ni. Fig. 6 shows Brillouine zone and Fig. 7 shows band structure of Ni. We

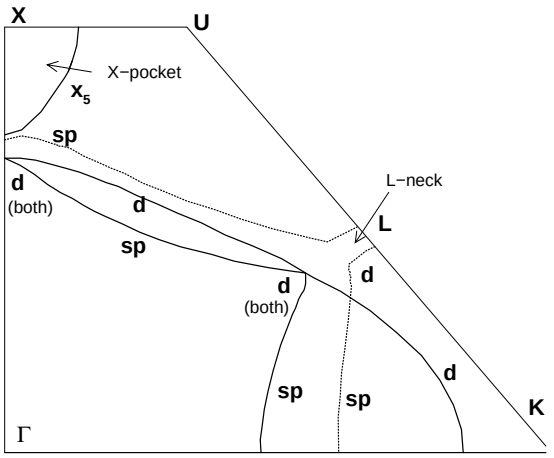

FIG. 8: Calculated Fermi Surface of Ni at $U = 1.9\,eV$ and $J = 1.2\,eV$. The solid and dotted lines correspond to majority and minority dominant spin carriers. Dominant orbital characters are expressed. Both experimentally confirmed X_5 pocket and L neck can be seen. The X_2 pocket is missing, which is in agreement with experiments.

now discuss the band structure at the Γ point. From the below we see three majority bands and three minority bands. The lowest one is dominated by $4sp$ orbital, the middle one is dominated by t_{2g} orbital, and the highest one is dominated by e_g orbital. In this paragraph, we call the bands by its dominant orbital character at the Γ point. The e_g band has two subbands. One of the two subbands is strongly hybridized with sp bands from the middle of the ΓX line. This band can be easily identified since the energy grows rapidly from the middle of the ΓX line and the rapidly growing part is dominated by sp orbitals. Inspecting the sp band, we observe that the band is rather flat at later part of the ΓX line. In this area, the band is dominated by e_g orbitals. The other subband of e_g band remains unhybridized along the ΓX line. The t_{2g} band has two subbands in the ΓX direction. One of the subbands is doubly degenerate and the other band is singlet. The doubly degenerate band can be identified by looking at the X point since this band breaks into two subbands there. Fig. 8 shows the Fermi surface deduced from the band structure.

We now discuss the band structure in relation with magnetic anisotropy. One important feature which emerges from the calculation is the absence of the X_2 pocket (see Fig. 8). This has been predicted by LDA but has not been found experimentally[33]. Inspecting the four band structures in band structure figures near the Fermi surface (Fig. 9), we notice that as we move away from the ΓX direction to ΓL direction, there is a band, which is above the Fermi surface at the X point, is submerged below the Fermi level. The band is the doubly degenerate t_{2g} subband and the pocket generated by this band is the experimentally confirmed X_5 pocket.

In the LDA band structure (see the top of Fig. 9),

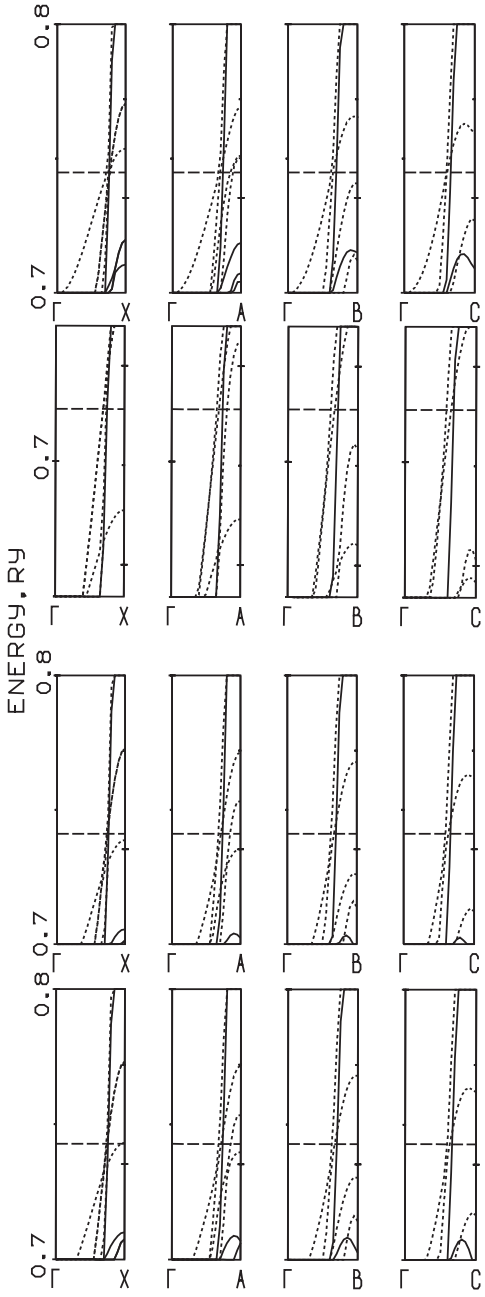

FIG. 9: The X pockets. From the top, band structure near X of LDA, LDA+U at $U = 4\ eV$ $J = 0\ eV$, LDA+U at $U = 1.9\ eV$ $J = 1.2\ eV$, and LDA+U at $U = 1.7\ eV$ $J = 1.1\ eV$. The size of the windows are 1 Ry. The solid lines represent bands with dominating up-spin. The dotted lines represent bands with dominating down-spin. $X = (0, 0, 1)$, $A = (1/16, 1/16, 1)$, $B = (2/16, 2/16, 1)$, $C = (3/16, 3/16, 1)$.

there is another band forming another X pocket. This is the unhybridized e_g subband and the pocket generated by this band is the LDA X_2 pocket. The LDA X_2 pocket has not been found experimentally. In LDA+U (see the second and the third of Fig. 9), the corresponding band is pushed down below the Fermi level and no X_2 pocket is present conforming to the experiments. This is

expected since correlation effects are more important for slower electrons and the velocity near the pocket is rather small. For the path with $J = 0$, we find that the removal of X_2 pocket is around $U = 3\ eV$ far off from $U = 4\ eV$ where the correct magnetic anisotropy is predicted. Notice that the corresponding band is way below the Fermi level at $U = 4\ eV$ (see the second of Fig. 9). For the path with the experimental magnetic moments, we also find that the removal of the X_2 point is near the point $U = 1.9\ eV$ and $J = 1.2\ eV$ where the correct magnetic anisotropy is predicted. A very important point to notice is that the band that makes X_2 pocket in LDA is just below the Fermi level (see the third of Fig. 9). This brings a suspicion that the point $U = 1.9\ eV$ and $J = 1.2\ eV$ is where the X_2 pocket just disappear. For this reason we study the X_2 pockets at $U = 1.7\ eV$ and $J = 1.1\ eV$ (see the bottom of Fig. 9). The corresponding band is just above the Fermi level forming a tiny pocket . This removal of X_2 pocket near the point where the correct magnetic anisotropy is predicted, strengthens the connection between MAE and the absence of X_2 pocket.

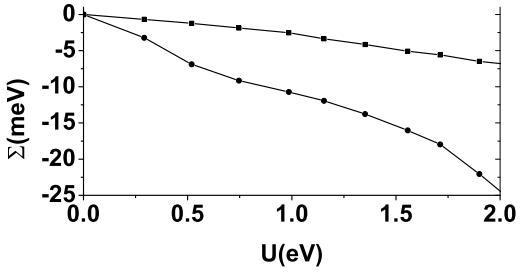

FIG. 10: Diagonal Components of Self energy matrix $\Sigma^{\downarrow\downarrow}_{aa}$ for minority spin. Notice that e_g band (circle) is more pushed down than t_{2g} band (square)

This disappearance of X_2 pocket can be explained in terms of self energy $\Sigma^{\sigma\sigma'}_{ab}$. For simplicity, we consider only diagonal components. Due to the cubic symmetry, these diagonal components are the same for orbitals in t_{2g} band and for orbitals in e_g band:

$$\Sigma^{\sigma\sigma}_{aa} = \begin{cases} \Sigma^{\sigma}_{t_{2g}} & \text{for orbitals in } t_{2g} \text{ bands} \\ \Sigma^{\sigma}_{e_g} & \text{for orbitals in } e_g \text{ bands} \end{cases} \tag{37}$$

Since both X_2 pocket and X_5 bands are dominated by minority spins, we consider only minority spins here (see Fig. 10). At $U = 1.9\ eV$ and $J = 1.2\ eV$, we find that $\Sigma_{t_{2g}} = -0.09\ eV$ and $\Sigma_{e_g} = -0.30\ eV$. This shows that e_g bands are suppressed more by strong correlation than t_{2g} bands. Since X_2 pocket is dominated by e_g bands and X_5 pocket is dominated by t_{2g} bands, the X_2 pocket is removed by Strong correlation effects while X_5 pocket survives. For comparison, we find that $\Sigma_{t_{2g}} = -0.04\ eV$ and $\Sigma_{e_g} = -0.15\ eV$ at $U = 1.1\ eV$ and $J = 0.64\ eV$

There has been some suspicions that the incorrect position of the X_2 band within LDA was responsible for the incorrect prediction of the easy axis within this theory. Daalderop and coworkers[11] removed the X_2 pocket by increasing the number of valence electrons and found the correct easy axis. We therefore conclude that the absence of the pocket is one of the central elements in determining the magnetic anisotropy, and there is no need for any ad-hoc adjustment within a theory which takes into account the correlations.

We now describe the effects originated from (near) degenerate states close to the Fermi surface. These have been of primary interest in past analytic studies[6,7]. We will call such states *degenerate Fermi surface crossing* (DFSC) states. The contribution to MAE by non-DFSC states comes from the fourth order perturbation. Hence it is of the order of λ^4, where λ is spin–orbit coupling constant. The energy splitting between DFSC states due to spin-orbit coupling is of the order of λ because the contribution comes from the first order perturbation. Using linear approximation of the dispersion relation $\epsilon(\vec{k}\lambda)$, the relevant volume in k-space was found of the order λ^3. Thus, these DFSC states make contribution of the order of λ^4. Moreover, there may be accidentally near DFSC states appearing along a line on the Fermi surface, rather than at a point. We have found this to be the case in our LDA calculation for Ni. Therefore the contribution of DFSC states is as important as the bulk non-DFSC states though the degeneracies occur only in small portion of the Brillouine zone.

This importance of the DFSC states leads us to comparative analysis of the LDA and LDA+U band structures near the Fermi level. In LDA (see top of Fig. 9), five bands are crossing the Fermi level at nearly the same points along the ΓX direction. Two of the five bands are degenerate for the residual symmetry and the other three bands accidentally cross the Fermi surface at nearly the same points. There are two sp bands with spin up and spin down, respectively. The other three bands are dominated by d orbitals. In LDA+U (see second and third of Fig. 9), one of the d bands is pushed down below the Fermi surface. The other four bands are divided into two degenerate pieces at the Fermi level (see Fig. 9): Two symmetry related degenerate $d_\downarrow$ bands and two near degenerate $sp_\uparrow$ and $sp_\downarrow$ bands. In sum the correlation weakens the effect of degenerate bands along ΓX direction.

In LDA (see the top of Fig. 9), we found that two bands are accidentally near degenerate along the line on the Fermi surface within the plane ΓXL. One band is dominated by $d_\downarrow$ orbitals. The other is dominated by $d_\downarrow$ orbitals near X and by $s_\downarrow$ orbitals off X. This accidental DFSC states persist from ΓX direction to ΓL direction. (Along ΓL direction, the degeneracy is for the residual symmetry). In LDA+U, these accidental DFSC states disappear(see Fig. 8). With the correlation effect U, this accidental DFCS states along a line on the Fermi surface move away from the Fermi surface leaving only the states along ΓL direction DFSC. This degenerate states' moving away from Fermi surface makes the first order perturbation effect sums up to zero.

FIG. 11: The L neck of LDA+U at $U = 1.9\ eV$ $J = 1.2\ eV$. Notice the absence of L pockets. nspecting the figures, we see that there is a L neck. The solid lines represent bands with dominating up-spin. The dotted lines represent bands with dominating down-spin. The horizontal line is the Fermi level. The points are: $N = (29/64, 29/64, 19/32)$, $O = (30/64, 30/64, 18/32)$, $P = (31/64, 31/64, 17/32$, $Q = (125/256, 125/256, 67/128)$, $R = (126/256, 126/256, 66/128)$, $S = (127/256, 127/256, 65/128)$, $L = (128/256, 128/256, 64/128)$.

We now discuss another feature of Fermi surface, that is the L neck. The experimental L neck is a spin-up dominated band. From the Fig. 11, we see one spin-up dominated band is just below the Fermi level in ΓL direction. As we move away from the ΓL direction, we see that the band is surfacing up above the Fermi level. This is the experimentally confirmed L neck. This L neck can be found at both $(U, J) = (1.9\ eV, J = 1.2\ eV)$ and $(U, J) = (4.0\ eV, J = 0\ eV)$. For $(U, J) = (4.0\ eV, J = 0\ eV)$, we find additional L pockets that has not been found in experiments.

Based on the tight–binding model, the importance of DFSC states has been shown[6,7]. We see that strong correlations reduce number of DFSC states in ΓX direction and remove the near degenerate states on ΓXL plane. We conclude that the change of DFSC states is another important element that determines the easy axis of Ni. The correct configuration is tantamount to the correct Fermi surface. We see that it is possible to find the correct Fermi surface at $U = 1.9\ eV$ and $J = 1.2\ eV$ where the magnetic moment and magnetic anisotropy can be correctly predicted. A point to note is that the Fermi surface does not come out right for other points in (U, J) parameter space.

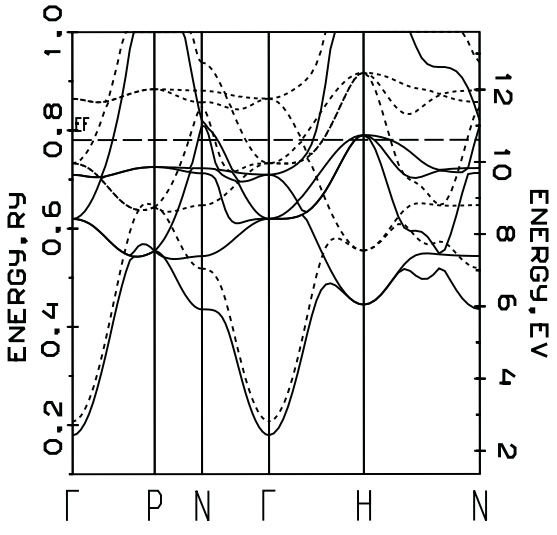

FIG. 12: The band structure of Fe for LDA.

Now we discuss band structure of Fe. Unlike Ni, strong correlation effects do not change bands structure of Fe near the Fermi surface significantly (see Fig. 12 and 13). Most of the minority spin d bands lie above the Fermi surface and the self energy is not large enough to push the bands down near the Fermi surface. This is very different situation from that of Ni, where minority spin d bands are near the Fermi surface and the self energy is of comparable magnitude. The self energy of minority spin e_g band is positive for Fe. Since most of this band lies above the Fermi surface, the effects of strong correlation to occupied states is insignificant. Majority spin d bands lie far below the Fermi level. Since the self energy for this band is negative, the bands are pushed down more by strong correlations. This is the same situation as that of Ni and there is no significant changes near the Fermi level by strong correlations. The band structure of LDA and LDA+U are drawn in Fig. 12 and 13 . Comparing the two band structure, one can see that there is no significant change near the Fermi surface. This explains why magnetic anisotropy of Fe has been solved in LSDA while magnetic anisotropy of Ni needs a proper treatment of strong correlations.

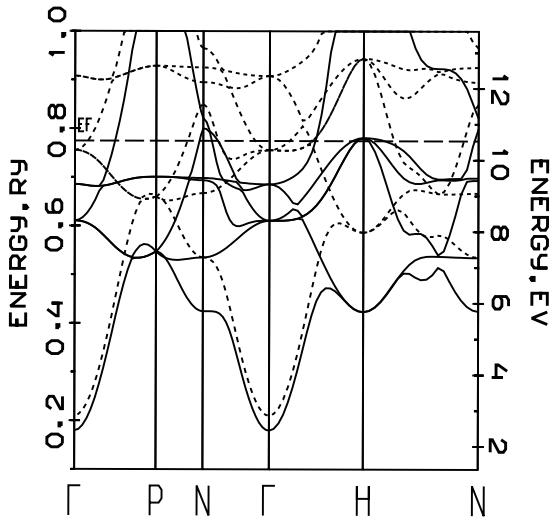

FIG. 13: The band structure of Fe for LDA+U at $U = 1.2\ eV$ and $J = 0.8\ eV$.

V. SPIN–OTHER–ORBIT COUPLING

Our implementation of relativistic effects neglects other relativistic corrections than spin–orbit coupling. In this section, we first present that other relativistic effect can be seamlessly incorporated into out approach, then discuss spin–other–orbit coupling, which might be important in calculating magnetic anisotropy energy.

We can divide relativistic corrections into one-body interactions and two-body interactions. One-body interactions are spin-orbit coupling, relativistic mass correction, and Darwin term. These one-body interactions can be in-

cluded into Kohn–Sham Hamiltonian in the same way as spin–orbit coupling is included. Only spin-orbit coupling terms is relevant to magnetic anisotropy energy and it has been the main theme of this paper.

There are two two-body interactions coming from relativistic corrections, spin–other–orbit coupling and spin–spin interaction:

$$H_{SOO} = -\frac{\mu_B^2}{2}\sum_{i<j}\frac{1}{r_{ij}^3}\hat{\mathbf{r}}_{ij}\times\mathbf{p}_i\cdot(\mathbf{s}_i+2\mathbf{s}_j), \quad (38)$$

$$H_{SS} = \frac{\mu_B^2}{2}\sum_{i<j}\frac{1}{r_{ij}^3}[\mathbf{s}_i\cdot\mathbf{s}_j-(\mathbf{r}_{ij}\cdot\frac{\mathbf{s}_i)(\mathbf{r}_{ij}\cdot\mathbf{s}_j)}{r_{ij}^2}]. \quad (39)$$

We now present the scheme of including two body interactions. A fermionic field operator Ψ can be expanded along orthonormal complete bases $\{\Phi_\alpha\}$ where α is a combined index:

$$\Psi=\sum_\alpha a_\alpha\Phi_\alpha. \quad (40)$$

In this bases, the canonical anti–commutator relation can be written down in creation and annihilation operators: $\{a_\alpha^\dagger,a_\beta\}=\delta_{\alpha\beta}$. In second quantization approach, any two particle interaction can be written down as

$$H_{\rm int}=\frac{1}{2}\sum_{\alpha\beta\gamma\delta}a_\alpha^\dagger a_\gamma^\dagger a_\delta a_\beta U^{\alpha\beta\gamma\delta}, \quad (41)$$

The matrix element $U_{\alpha\beta\gamma\delta}$ can be found by

$$U_{\alpha\beta\gamma\delta}=\int\Phi_\alpha^\dagger(\mathbf{r}_1)\Phi_\gamma^\dagger(\mathbf{r}_2)v(1,2)\Phi_\delta(\mathbf{r}_2)\Phi_\beta(\mathbf{r}_1)d\mathbf{r}_1d\mathbf{r}_2, \quad (42)$$

where $v(1,2)$ is a two particle interaction between particle 1 and particle 2. The expectation value of $H_{\rm int}$ can expressed as

$$\langle H_{\rm int}\rangle=\sum_{\alpha\beta\gamma\delta}(n_{\alpha\beta}n_{\gamma\delta}-n_{\alpha\delta}n_{\gamma\beta})U^{\alpha\beta\gamma\delta}. \quad (43)$$

Introducing another interaction matrix

$$J_{\alpha\beta\gamma\delta}=\int\Phi_\alpha^\dagger(\mathbf{r}_1)\Phi_\gamma^\dagger(\mathbf{r}_2)v(1,2)\Phi_\beta(\mathbf{r}_2)\Phi_\delta(\mathbf{r}_1)d\mathbf{r}_1d\mathbf{r}_2, \quad (44)$$

The Eq. 43 can be written as

$$\langle H_{\rm int}\rangle=\sum_{\alpha\beta\gamma\delta}(U^{\alpha\beta\gamma\delta}-J^{\alpha\beta\gamma\delta})n_{\alpha\beta}n_{\gamma\delta}. \quad (45)$$

The approach described in section II can be straightforwardly extended to accommodate general two particle interactions by allowing spin dependent interaction matrices $U^{\alpha\beta\gamma\delta}$ and $J^{\alpha\beta\gamma\delta}$. Therefore, all the relativistic corrections can be included in the framework of DMFT and its static limit LDA+U.

The Coulomb interaction we have considered is one of the two particle interaction. In case of Coulomb interaction the interaction matrix $U_{\alpha\beta\gamma\beta}$ is independent of spin. For more rigorous discussion we decompose the index α to (a,σ), where σ is spin index and a contains all the others. The interaction matrix of Coulomb interaction is

$$U_{\alpha\beta\gamma\beta} = U_{abcd}\delta_{\sigma_a\sigma_b}\delta_{\sigma_c\sigma_d} \quad (46)$$

$$J_{\alpha\beta\gamma\beta} = J_{abcd}\delta_{\sigma_a\sigma_d}\delta_{\sigma_c\sigma_b}. \quad (47)$$

The U_{abcd} and J_{abcd} interaction matrices are the same interaction matrices in Eq. 16.

For general two particle interaction, the self energy is for spin-diagonal elements

$$\begin{aligned}\Sigma_{ab}^{\sigma\sigma} &= \sum_{cd}(U_{abcd}^{\sigma\sigma-\sigma-\sigma}-J_{abcd}^{\sigma\sigma-\sigma-\sigma})n_{cd}^{-\sigma-\sigma} \quad (48)\\ &+ \sum_{cd}(U_{abcd}^{\sigma\sigma\sigma\sigma}-J_{abcd}^{\sigma\sigma\sigma\sigma})n_{cd}^{\sigma\sigma}\\ &+ \sum_{cd}(U_{abcd}^{\sigma\sigma\sigma-\sigma}-J_{abcd}^{\sigma\sigma\sigma-\sigma})n_{cd}^{\sigma-\sigma}\\ &+ \sum_{cd}(U_{abcd}^{\sigma\sigma-\sigma\sigma}-J_{abcd}^{\sigma\sigma-\sigma\sigma})n_{cd}^{-\sigma\sigma}\\ &- \frac{\delta\Phi_{DC}}{\delta G_{ab}^{\sigma\sigma}(i\omega)}.\end{aligned}$$

Unlike the case of Coulomb interaction, the spin–diagonal elements of self energy can get contributions from spin–off-diagonal density matrix components. Notice that there are contributions from spin-diagonal elements with opposite spin through exchange interaction ($J_{abcd}^{\sigma\sigma-\sigma-\sigma}n_{cd}^{-\sigma-\sigma}$). The spin off–diagonal elements of self energy $\Sigma_{ab}^{\sigma-\sigma}$ takes the same form as the spin-diagonal elements except that the spin corresponding to the index b is $-\sigma$ instead of σ.

We now study spin–other–orbit coupling. In this interaction, the spin degrees of freedom sees spatial anisotropy through orbital degrees of freedom. Spin–other-orbit coupling, therefore, may be important in magnetic anisotropy, though its contribution to MAE might be small. Since each term in spin-other-orbit coupling contains only one spin operator, either spins of α and β or spins of γ and δ must be the same in Eq. 43. Using this observation, the spin-diagonal elements of self energy is simplified to

$$\begin{aligned}\Sigma_{ab}^{\sigma\sigma} &= \sum_{cd}(U_{abcd}^{\sigma\sigma-\sigma-\sigma})n_{cd}^{-\sigma-\sigma} \quad (49)\\ &+ \sum_{cd}(U_{abcd}^{\sigma\sigma\sigma\sigma}-J_{abcd}^{\sigma\sigma\sigma\sigma})n_{cd}^{\sigma\sigma}\\ &+ \sum_{cd}(U_{abcd}^{\sigma\sigma\sigma-\sigma}-J_{abcd}^{\sigma\sigma\sigma-\sigma})n_{cd}^{\sigma-\sigma}\\ &+ \sum_{cd}(U_{abcd}^{\sigma\sigma-\sigma\sigma}-J_{abcd}^{\sigma\sigma-\sigma\sigma})n_{cd}^{-\sigma\sigma}\\ &- \frac{\delta\Phi_{DC}}{\delta G_{ab}^{\sigma\sigma}(i\omega)},.\end{aligned}$$

Notice that the contribution from spin-diagonal density matrix components has the same form as the one of

Coulomb interaction except that $U^{\sigma\sigma\sigma\sigma}_{abcd}$ need not to be the same as $U^{\sigma\sigma-\sigma-\sigma}_{abcd}$. Since the spin-off-diagonal density matrix elements are small compared to the spin-diagonal elements, we may neglect such contributions. When Coulomb interaction is consider as well as spin–other interaction, its contribution to the interaction matrix elements of the form $U^{\sigma\sigma\sigma\sigma}_{abcd}$, $U^{\sigma\sigma-\sigma-\sigma}_{abcd}$, or $J^{\sigma\sigma\sigma\sigma}_{abcd}$ is much larger than that of spin–other–coupling. In this approximation, the contribution of spin–other–orbit coupling is negligible and the spin-diagonal elements of self energy is then the same as that of Coulomb interaction.

Spin off–diagonal elements is given by

$$\begin{aligned}\Sigma^{\sigma-\sigma}_{ab} &= \sum_{cd}(-J^{\sigma-\sigma-\sigma\sigma}_{abcd})n^{-\sigma\sigma}_{cd} \\ &+ \sum_{cd}(U^{\sigma-\sigma-\sigma-\sigma}_{abcd} - J^{\sigma-\sigma-\sigma-\sigma}_{abcd})n^{-\sigma-\sigma}_{cd} \quad (50)\\ &+ \sum_{cd}(U^{\sigma-\sigma\sigma\sigma}_{abcd} - J^{\sigma-\sigma\sigma\sigma}_{abcd})n^{\sigma\sigma}_{cd} \\ &- \frac{\delta\Phi_{DC}}{\delta G^{\sigma-\sigma}_{ab}(i\omega)}.\end{aligned}$$

The contributions from spin–off–diagonal density matrix elements has the same from as that of Coulomb interaction. Notice that there are contributions from spin–diagonal density matrix elements. This contribution should be treated on the same footing as the contributions from spin–off–diagonal density matrix elements, hence the correction from spin–other–orbit coupling is not negligible. For an extensive study of this effect, we need an implementable formula. We developed an formula that can be implemented in Appendix

An extensive study on the effects of spin–other–coupling to spin–off–diagonal elements of self energy requires another paper. Instead, we estimate the order of magnitude of spin–other–orbit coupling here. The order of magnitude of spin–other–coupling can be estimated by using $\langle 1/r^3_{ij}\rangle \sim \langle 1/r_{ij}\rangle^3$ to $(CI/2\alpha mc^2)^2 CI$, where CI is the strength of Coulomb interaction and α is the fine structure constant. We see that the order of magnitude of CI is 1 eV for d shell electrons of Ni and Fe. Therefore, the spin–other–interaction is 10^{-8} times smaller than the Coulomb interaction. The effect of spin–other–orbit coupling is, therefore negligible. This has been confirmed by the study of Stiles and coworkers[34].

VI. CONCLUSION

We have studied the effects of strong correlations on magnetic anisotropy. We find that magnetic anisotropy changes as correlation strength U and J change. These has been shown along several paths in (U, J) space. The correct magnetic anisotropy can be predicted at several points in (U, J) space for both Ni and Fe. Moreover, magnetic moment, magnetic anisotropy, and Fermi surface are correctly predicted simultaneously at physically acceptable values of U and J: $U = 1.9\,eV$ and $J = 1.2\,eV$ for Ni and $U = 1.2\ eV$ and $J = 0.8\ eV$ for Fe.

It is remarkable that the values of U necessary to reproduce the correct magnetic anisotropy energy are very close (within 1.2 eV) to the values which are needed to describe photoemission spectra of these materials[35,36]. The correct estimation of U is indeed a serious problem. Different estimates based on different methods give a range of values from 1 eV to 6 eV. The work of Katsnelson and coworkers used a dynamic approach utilizing finite temperature Quantum Monte Carlo method whereas we use a static approach at zero temperature. Considering these discrepancies, an agreement within $1.2eV$ shows an internal consistency of our approach and emphasizes the importance of correlations.

For Ni, we find that the LDA X_2 pocket disappears near $U = 1.9\ eV$ and $J = 1.2\ eV$ where the correct magnetic moment and the correct magnetic anisotropy are predicted simultaneously. This suggests a tight relation between the absence of X_2 pocket and the correct magnetic anisotropy as suggested by previous work. The change of DFSC states from LDA to LDA+U is discussed. DFSC states are old suspects of dominant contribution to magnetic anisotropy. The correct configuration of DFSC states and the absence of X_2 pocket are by-products of the correct Fermi surface that we predict for the first time. For Fe, we find that strong correlations do not change band structures significantly. This is attributed to the fact that most of minority bands lie above the Fermi level, hence the change of band structures has no large effect to occupied states. This distinguishes the magnetic anisotropy problem for Fe from the one for Ni.

The calculations performed are state of the art in what can currently be achieved for realistic treatments of correlated solids. Despite the great successes of the LDA+U theory in predicting material properties of correlated solids (for a review, see book of Anisimov[19]), there are obvious problems of this approach when applied to metals or to systems where the orbital symmetries are not broken. The most noticeable is that it only describes spectra which has Hubbard bands. A correct treatment of the electronic structure of strongly correlated electron systems has to treat both Hubbard bands and quasiparticle bands on the same footing. Another problem occurs in the paramagnetic phase of Mott insulators, in the absence of any broken symmetry the LDA + U method reduces to the LDA, and the gap collapses. In systems like NiO where the gap is of the order of eV, but the Neel temperature is a few hundred Kelvin, it is unphysical to assume that the gap and the magnetic ordering are related. For this reason the LDA+U predicts magnetic order in cases that it is not observed, as, e.g., in the case of Pu[37]. Since LDA+U method is a limiting case of more general DMFT, these difficulties are expected to be overcome in DMFT. Further studies should be devoted to improving the quality of the solution of the impurity model within DMFT and extending the calculation to finite temperatures.

Acknowledgments

This research was supported by the ONR grants No. 4-2650 and N00014-02-1-0766. GK would like to thank K. Hathaway for discussing the origin of magnetic anisotropy and G. Lonzarich for discussing dHvA data. We thank R. Chitra for stimulating discussions. We thank V. Oudovenko and C. Uebing for developing and setting up the Beowulf computer cluster used to perform these calculations. We have also used the supercomputer at the Center for Advanced Information Processing, Rutgers.

APPENDIX

In this appendix, we develop an computationally implementable formula for spin–other–orbit coupling:

$$v(1,2) = i\mu_B^2 \frac{(\mathbf{r}_1 - \mathbf{r}_2)\times\nabla_1}{r_{12}^3}\cdot(\sigma_1 + 2\sigma_2) + 1 \leftrightarrow 2, \quad (51)$$

where σ_1 applies to states at $\mathbf{r}_1$ and σ_2 to states at $\mathbf{r}_2$. For simplicity, we will only work the first term out. The formula for the second term can be found by exchanging 1 and 2. Using the identity

$$\nabla = \hat{\mathbf{r}}\frac{\partial}{\partial r} - i\frac{\mathbf{r}\times\vec{L}}{r^2}, \quad (52)$$

the spin-other-interaction can be written down as

$$\begin{aligned} v(1,2) &= -\mu_B^2 \frac{1}{r_{12}^3}\vec{L}_1\cdot(\sigma_1+2\sigma_2) \quad (53)\\ &+ i\mu_B^2 r_2 \frac{(\hat{\mathbf{r}}_1)\times\hat{\mathbf{r}}_2}{r_{12}^3}\cdot(\sigma_1+2\sigma_2)\frac{\partial}{\partial r_1}\\ &- \mu_B^2\frac{r_2}{r_1}\frac{\hat{\mathbf{r}}_2\cdot\hat{\mathbf{r}}_1}{r_{12}^3}\vec{L}_1\cdot(\sigma_1+2\sigma_2)\\ &+ \mu_B^2\frac{r_2}{r_1}\frac{\hat{\mathbf{r}}_2\cdot\vec{L}_1}{r_{12}^3}\hat{\mathbf{r}}_1\cdot(\sigma_1+2\sigma_2). \end{aligned}$$

We will write the interaction matrix as

$$U_{\alpha\beta\gamma\delta} = U^1_{\alpha\beta\gamma\delta} + U^2_{\alpha\beta\gamma\delta} + U^3_{\alpha\beta\gamma\delta}, \quad (54)$$

where $U^1_{\alpha\beta\gamma\delta}$ comes from the first term, $U^2_{\alpha\beta\gamma\delta}$ from the second term, and $U^3_{\alpha\beta\gamma\delta}$ from the third and fourth terms of the Eq. 54. For easiness of following index structure, we define the interaction matrix U as

$$U_{\alpha\beta\gamma\delta} = \int \Phi^\dagger_\alpha(\mathbf{r}_1)\Phi^\dagger_\beta(\mathbf{r}_2)v(1,2)\Phi_\gamma(\mathbf{r}_2)\Phi_\delta(\mathbf{r}_1)d\mathbf{r}_1 d\mathbf{r}_2. \quad (55)$$

We will consider bases in the from of

$$\Phi_{ilm\sigma}(\mathbf{r}) = \phi_{il}(r)Y_{lm}(\theta,\phi)\chi_\sigma, \quad (56)$$

where $\chi_\sigma = (1,0)^T$, or $(0,1)^T$. Note that the angles θ and ϕ is measured with respect to the origin of a coordinate system.

We want to separate the spin-other-orbit interaction into radial part and angular part. This can be done by using the following property

$$\frac{1}{r_{12}^3} = \sum_{lm} f_l(r_1,r_2)Y^*_{lm}(\theta_2,\phi_2)Y_{lm}(\theta_1,\phi_1), \quad (57)$$

where

$$f_l(r_1,r_2) = 4\pi\int_{-1}^{1}\frac{P_l(x)}{(r_1^2+r_2^2-2r_1r_2x)^{2/3}}dx. \quad (58)$$

For example we write down f_0 and f_1 explicitly:

$$f_0(r_1,r_2) = \frac{4\pi}{r_1r_2}[\frac{1}{|r_1-r_2|} - \frac{1}{r_1+r_2}] \quad (59)$$

$$\begin{aligned} f_1(r_1,r_2) = \frac{2\pi}{r_1^2r_2^2}[&\frac{(r_1-r_2)^2+r_1^2+r_2^2}{|r_1-r_2|}\\ &-\frac{(r_1+r_2)^2+r_1^2+r_2^2}{r_1+r_2}]. \quad (60) \end{aligned}$$

With these identities, we can calculate a readily implementable formula for spin–other–orbit interaction. After some manipulation, we can write the contribution from the first terms of the Eq. 54 as

$$\begin{aligned} &U^1_{(i_1l_1m_1\sigma_1)(i_2l_2m_2\sigma_2)(i_3l_3m_3\sigma_3)(i_4l_4m_4\sigma_4)}\\ =\ & -\mu_B^2\sum_{lm}\int dr_1dr_2f_l(r_1,r_2)\times\\ &\phi^*_{i_1l_1}(r_1)\phi^*_{i_2l_2}(r_1)\phi_{i_3l_3}(r_1)\phi_{i_4l_4}(r_1)\times\\ &\langle l_2m_2|Y_{lm}|l_3m_3\rangle\langle l_1m_1|Y_{lm}O_{\sigma_1\sigma_2\sigma_3\sigma_4}|l_4m_4\rangle, \quad (61) \end{aligned}$$

where the operator $O^1_{\sigma_1\sigma_2\sigma_3\sigma_4}$ is defined by

$$O^1_{\sigma_1\sigma_2\sigma_3\sigma_4} = 2\delta_{\sigma_1\sigma_4}O^1_{\sigma_2\sigma_3} + \delta_{\sigma_2\sigma_3}O^1_{\sigma_1\sigma_4} \quad (62)$$

$$\begin{aligned} O^1_{\uparrow\uparrow} &= L_z\\ O^1_{\downarrow\downarrow} &= -L_z\\ O^1_{\uparrow\downarrow} &= L_-\\ O^1_{\downarrow\uparrow} &= L_+ \end{aligned}$$

The contribution from the second terms of the Eq. 54 reads

$$\begin{aligned} &U^2_{(i_1l_1m_1\sigma_1)(i_2l_2m_2\sigma_2)(i_3l_3m_3\sigma_3)(i_4l_4m_4\sigma_4)} =\\ &i\mu_B^2\sum_{lm}\int dr_1dr_2r_2f_l(r_1,r_2)\times\\ &\phi^*_{i_1l_1}(r_1)\phi^*_{i_2l_2}(r_1)\phi_{i_3l_3}(r_1)\frac{\partial}{\partial r_1}\phi_{i_4l_4}(r_1)\times\\ &O^2_{(l_1m_1\sigma_1)(l_2m_2\sigma_2)(l_3m_3\sigma_3)(l_4m_4\sigma_4)}(lm), \quad (63) \end{aligned}$$

where

$$\begin{aligned} &O^2_{(l_1m_1\sigma_1)(l_2m_2\sigma_2)(l_3m_3\sigma_3)(l_4m_4\sigma_4)}(lm)\\ &= 2\delta_{\sigma_1\sigma_4}N^{\sigma_2\sigma_3}_{(l_1m_1)(l_2m_2)(l_3m_3)(l_4m_4)}(lm)\\ &+\delta_{\sigma_2\sigma_3}N^{\sigma_1\sigma_4}_{(l_1m_1)(l_2m_2)(l_3m_3)(l_4m_4)}(lm), \quad (64) \end{aligned}$$

and the operator $N^{\sigma_1\sigma_2}_{(l_1m_1)(l_2m_2)(l_3m_3)(l_4m_4)}(lm)$ is defined as

$$N^{\uparrow\uparrow}_{(l_1m_1)(l_2m_2)(l_3m_3)(l_4m_4)}(lm) = A^z_{(l_1m_1)(l_2m_2)(l_3m_3)(l_4m_4)}(lm) \quad (65)$$

$$N^{\downarrow\downarrow}_{(l_1m_1)(l_2m_2)(l_3m_3)(l_4m_4)}(lm) = -A^z_{(l_1m_1)(l_2m_2)(l_3m_3)(l_4m_4)}(lm) \quad (66)$$

$$N^{\uparrow\downarrow}_{(l_1m_1)(l_2m_2)(l_3m_3)(l_4m_4)}(lm) = A^-_{(l_1m_1)(l_2m_2)(l_3m_3)(l_4m_4)}(lm) \quad (67)$$

$$N^{\downarrow\uparrow}_{(l_1m_1)(l_2m_2)(l_3m_3)(l_4m_4)}(lm) = A^+_{(l_1m_1)(l_2m_2)(l_3m_3)(l_4m_4)}(lm). \quad (68)$$

The operator $\vec{A}_{(l_1m_1)(l_2m_2)(l_3m_3)(l_4m_4)}(lm)$ is defined by a cross product of another operator $\vec{B}_{(l_1m_1)(l_2m_2)}$:

$$\vec{A}_{(l_1m_1)(l_2m_2)(l_3m_3)(l_4m_4)}(lm) = \vec{B}_{(l_1m_1)(l_4m_4)}(lm) \times \vec{B}_{(l_2m_2)(l_3m_3)}(lm), \quad (69)$$

where

$$B^x_{lml'm'}(lm) = \sqrt{\frac{2\pi}{3}}\langle lm|Y_{lm}(Y_{1-1} - Y_{11})|l'm'\rangle \quad (70)$$

$$B^y_{lml'm'}(lm) = \sqrt{\frac{2\pi}{3}}\langle lm|Y_{lm}(Y_{1-1} + Y_{11})|l'm'\rangle \quad (71)$$

$$B^z_{lml'm'}(lm) = \sqrt{\frac{4\pi}{3}}\langle lm|Y_{lm}Y_{10}|l'm'\rangle \quad (72)$$

The contribution from the last two terms of the Eq. 54 is

$$U^3_{(i_1l_1m_1\sigma_1)(i_2l_2m_2\sigma_2)(i_3l_3m_3\sigma_3)(i_4l_4m_4\sigma_4)} = \mu_B^2 \sum_{lm}\int dr_1 dr_2 \frac{r_2}{r_1} f_l(r_1,r_2) \times \phi^*_{i_1l_1}(r_1)\phi^*_{i_2l_2}(r_1)\phi_{i_3l_3}(r_1)\phi_{i_4l_4}(r_1) \times \left[\frac{4\pi}{3}O^3_{(l_1m_1\sigma_1)(l_2m_2\sigma_2)(l_3m_3\sigma_3)(l_4m_4\sigma_4)}(lm) - \frac{2\pi}{3}O^4_{(l_1m_1\sigma_1)(l_2m_2\sigma_2)(l_3m_3\sigma_3)(l_4m_4\sigma_4)}(lm)\right]. \quad (73)$$

The operator $O^3_{(l_1m_1\sigma_1)(l_2m_2\sigma_2)(l_3m_3\sigma_3)(l_4m_4\sigma_4)}(lm)$, which represents the contribution from the third term, is defined by

$$\begin{aligned} &O^3_{(l_1m_1\sigma_1)(l_2m_2\sigma_2)(l_3m_3\sigma_3)(l_4m_4\sigma_4)}(lm) \\ &= \langle l_2m_2|Y_{lm}Y_{10}|l_3m_3\rangle \times \\ &\langle l_1m_1|Y_{lm}Y_{10}O^1_{\sigma_1\sigma_2\sigma_3\sigma_4}|l_4m_4\rangle \\ &-\langle l_2m_2|Y_{lm}Y_{11}|l_3m_3\rangle \times \\ &\langle l_1m_1|Y_{lm}Y_{1-1}O^1_{\sigma_1\sigma_2\sigma_3\sigma_4}|l_4m_4\rangle \\ &-\langle l_2m_2|Y_{lm}Y_{1-1}|l_3m_3\rangle \times \\ &\langle l_1m_1|Y_{lm}Y_{11}O^1_{\sigma_1\sigma_2\sigma_3\sigma_4}|l_4m_4\rangle, \end{aligned} \quad (74)$$

where $O^1_{\sigma_1\sigma_2\sigma_3\sigma_4}$ is given by the Eq. 62. The operator $O^4_{(l_1m_1\sigma_1)(l_2m_2\sigma_2)(l_3m_3\sigma_3)(l_4m_4\sigma_4)}(lm)$ which represents the contribution from the last term, is defined by

$$\begin{aligned} &O^4_{(l_1m_1\sigma_1)(l_2m_2\sigma_2)(l_3m_3\sigma_3)(l_4m_4\sigma_4)}(lm) \\ &= \sqrt{2}\langle l_2m_2|Y_{lm}Y_{10}|l_3m_3\rangle \times \\ &\langle l_1m_1|Y_{lm}O^4_{\sigma_1\sigma_2\sigma_3\sigma_4}L_z|l_4m_4\rangle \\ &-\langle l_2m_2|Y_{lm}Y_{11}|l_3m_3\rangle \times \\ &\langle l_1m_1|Y_{lm}O^4_{\sigma_1\sigma_2\sigma_3\sigma_4}L_-|l_4m_4\rangle \\ &-\langle l_2m_2|Y_{lm}Y_{1-1}|l_3m_3\rangle \times \\ &\langle l_1m_1|Y_{lm}O^4_{\sigma_1\sigma_2\sigma_3\sigma_4}L_+|l_4m_4\rangle, \end{aligned} \quad (75)$$

where $O^4_{\sigma_1\sigma_2\sigma_3\sigma_4}$ is given by the following equations:

$$O^4_{\sigma_1\sigma_2\sigma_3\sigma_4} = 2\delta_{\sigma_1\sigma_4}O^4_{\sigma_2\sigma_3} + \delta_{\sigma_2\sigma_3}O^4_{\sigma_1\sigma_4} \quad (76)$$

$$\begin{aligned} O^1_{\uparrow\uparrow} &= \sqrt{2}Y_{10} \\ O^1_{\downarrow\downarrow} &= -\sqrt{2}Y_{10} \\ O^1_{\uparrow\downarrow} &= Y_{1-1} \\ O^1_{\downarrow\uparrow} &= -Y_{11}. \end{aligned}$$

* Electronic address: iyang@physics.rutgers.edu
† Electronic address: serguei.savrassov@njit.edu; URL: http://physics.njit.edu/~savrasov
‡ Electronic address: kotliar@physics.rutgers.edu; URL: http://www.physics.rutgers.edu/~kotliar

[1] J. H. van Vleck, Phys. Rev. **52**, 1178 (1937).
[2] H. Brooks, Phys. Rev. **58**, 909 (1940).
[3] G. C. Fletcher, Proc. R. Soc. London **67A**, 505 (1954).
[4] J. C. Sloncewskij, J. Phys. Soc. Jpn. **17**, Suppl. B (1962).
[5] M. Asdente and M. Delitala, Phys. Rev. **163**, 497 (1967).
[6] E. I. Kondorskii and E. Straube, Sov. Phys.-JETP **36**, 188 (1973).
[7] N. Mori, Y. Fukuda, and T. Ukai, J. Phys. Soc. Jpn. **37**, 1263 (1974).
[8] P. Hohenberg and W. Kohn, Phys. Rev. **136**, 864 (1964).
[9] O. Gunnarson and B. I. Lundqvist, Phys. Rev. B **13**, 4274 (1976).
[10] H. Eckardt, L. Fritsche, and J. Noffke, J. Phys. F **17**, 943 (1987).
[11] G. H. O. Daalderop, P. J. Kelly, and M. F. H. Schuurmans, Phys. Rev. B **41**, 11 919 (1990).
[12] A. Mackintosh and O. K. Andersen, in *Electronsat Fermi Surface*, edited by M. Springford (Cambridge University Press, Cambridge, England, 1980).
[13] D. Wang, R. Wu, and A. J. Freeman, Phys. Rev. Lett. **70**, 869 (1993).
[14] J. Trygg, B. Johansson, O. Eriksson, and J. M. Willis, Phys. Rev. Lett. **75**, 2871 (1995).

[15] H. J. F. Jansen, J. Appl. Phys. **67**, 4555 (1990).
[16] G. Schneider, R. P. Erickson, and H. J. F. Jansen, J. Appl. Phys. **81**, 3869 (1997).
[17] S. Halilov and *et al.*, Phys. Rev. B **57**, 9557 (1998).
[18] A. Georges, G. Kotliar, W. Krauth, and M. Rozenberg, Rev. Mod. Phys. **68**, 13 (1996).
[19] *Strong Correlations in electronic structure calculations*, edited by V. I. Anisimov (Gordon and Breach Science Publishers, Amsterdam, 2000).
[20] L. Nordstrom and D. Singh, Phys. Rev. Lett. **76**, 4420 (1996).
[21] I. Yang, S. Y. Savrasov, and G. Kotliar, Phys. Rev. Lett. **87**, 6405 (2001).
[22] G. Kotliar and S. Y. Savrasov, To be published .
[23] R. Chitra and G. Kotliar, Phys. Rev. B **62**, 12715 (2000).
[24] O. K. Andersen, Phys. Rev. B **12**, 3060 (1975).
[25] D. D. Koelling and B. N. Harmon, J. Phys. C: Solid State Phys. **10**, 3107 (1977).
[26] V. I. Anisimov, F. Aryastiawan, and A. I. Lichtenstein, J. Phys.: Condensed Matter **9**, 767 (1997).
[27] V. I. Anisimov, J. Zaanen, and O. K. Andersen, Phys. Rev. B **44**, 943 (1991).
[28] S. Y. Savrasov, Phys. Rev. B **54**, 16470 (1996).
[29] S. Froyen, Phys. Rev. B **39**, 3168 (1989).
[30] M. Methfessel and A. T. Paxton, Phys. Rev. B **40**, 3616 (1989).
[31] M. B. Stearns, in *Landolt Börnstein New Series*, edited by K. H. Hellewege and O. Madelung (Springer-Verlag, Berlin, 1987), Vol. III.
[32] V. Drchal, V. Janis, and J. Kundrnovsky, Phys. Rev. B **60**, 15664 (1999).
[33] C. S. Wang and J. Callaway, Phys. Rev. B **9**, 4897 (1973).
[34] M. D. Stiles and *et al.*, Phys. Rev. B **64**, 104430 (2001).
[35] M. Katsenelson and A. Lichtenstein, J. Phys. Cond. Matt. **11**, 1037 (1999).
[36] M. Katsenelson and A. Lichtenstein, Phys. Rev. B **61**, 8906 (2000).
[37] S. Savrasov and G. Kotliar, Phys. Rev. Lett. **84**, 3670 (2000).